SYNTHESIS OF NOVEL HIGH PERFORMANCE POLYURETHANE NANOCOMPOSITES FROM CASTOR OIL AS RENEWABLE POLYOL: STUDY ON MECHANICAL, THERMAL AND BARRIER PROPERTIES

ALAA MASHJEL ALI

Thesis submitted in fulfillment of the requirements
for the award of the degree of Doctor of Philosophy in
Chemical Engineering (Advanced Materials)

Faculty of Chemical Engineering & Natural Resource
UNIVERSITI MALAYSIA PAHANG

April 2015

ABSTRACT

Polyurethane nanocomposite is one of the promising materials and attracts many researchers to explore its potential. This work is aimed to develop a series of polyurethanes (PUs) based on castor oil with polyols as a renewable resource incorporated with different types of nano-fillers (organic and inorganic) to study the improved physico-chemical behaviour of novel polyurethanes fabricated with organically modified clay and purified Multi-Walled Carbon Nanotubes (MWCNTs) nanofillers; forming nanocomposites film by an in-situ polymerization technique and assisted by ultrasonication mixed at various times. Toluene diisocyanate (TDI) and chain extender 1, 4-butane diol (BDO) were employed with polyols to produce COPUs-(Cloisite 30B / MWCNTs) nanocomposites. The amount of nanofillers was varied from 0% to 5% wt for Cloisite 30B and for MWCNTs, the nanofillers range from 0% to 1% wt. The synthesized PU nanocomposites were characterized for different physical properties such as mechanical and morphology changes, oxidative thermal stability as well as sample purity and surface area studies using the Fourier Transform Infrared Spectroscopy (FTIR), the Field Emission Scanning Electron Microscopy (FESEM), X-ray diffraction (XRD), Thermogravimetric analysis (TGA) and Differential Scanning Calorimetry (DSC). Surface area was studied using the Brunauer-Emmet-Teller (BET) technique and elemental ratios were investigated using energy dispersive X-ray analysis (EDX) with the attached equipment in FESEM spectroscopy. The barrier properties were investigated by looking at nitrogen permeability measurements using a membrane separation unit. The thermal and mechanical properties of the COPUs matrix were found significantly improved with the incorporation of organoclay and MWCNTs. The purified MWCNTs were proven to have higher compatibility compared to organoclay in polymer matrix at even low concentrations of MWCNTs (0.3%), as results achieved presented higher *d* spacing, mechanical and thermal properties as shown in different instrumental analyses compared to its counterpart, organoclay (3 wt %). Tensile properties showed an improvement of ~ 324% in tensile strength and a decrease of ~74% in elongation at break with 5 wt% organoclay, while COPUs - MWCNTs nanocomposites depicted a massive development in tensile strength and lowering down of elongation at break with 1wt% (~640% and ~ 80%). Thermal properties depicted an increase of 10-30 ^{o}C in COPUs–C30B nanocomposites, while a significant increase of degradation temperature (~ 50 ^{o}C) was observed in 0.3 wt% of MWCNTs in the COPUs matrix. A major permeability reduction (~25 % and ~ 50%) was attained with 5 wt% of organoclay and 0.5 wt% MWCNTs loaded nanocomposites, compared to pure COPUs. The optimization study was conducted using a response surface methodology (RSM) which included the Central composite design (CCD) with three factors; temperature, time and the amount of nanofillers. An increase in temperature and nanofillers amount favoured the nanocomposites polymerization up to a certain extent. The optimum tensile strength obtained was 1.997 MPa at temperature 90 ^{o}C and wt% 4.99% for clay and 2.207 MPa at temperature 90 ^{o}C and wt% 1% for MWCNTs respectively.

ABSTRAK

Nanokomposit Poliuretana adalah salah satu daripada bahan-bahan yang berpotensi dan menarik ramai penyelidik untuk menyinkap potensinya. Usaha ini bertujuan untuk membangunkan satu siri poliuretana (PUs) berasaskan minyak jarak dengan poliol sebagai sumber yang boleh diperbaharui dengan menggabungkannya bersama pelbagai jenis pengisi nano (organik dan bukan organik) bagi mengkaji pertambah baikkan tingkah laku fiziko-kimia poliuretana baru yang difabrikkan bersama pengisi nano tanah liat organik yang telah diubahsuai dan tiub nano pelbagai-dinding yang telah di tulenkan (MWCNTs); membentuk filem nanokomposit dengan teknik pempolimeran in-situ, dibantu oleh ultrasonikasi pada pelbagai masa. Toluena diisosianat (TDI) dan rantaian penyambung 1, 4-butana diol (BDO) digunakan dengan poliol untuk menghasilkan nanokomposit COPUs- (Cloisite 30B / MWCNTs). Jumlah pengisi nano diubah daripada 0% hingga 5% berat (Cloisite 30B) dan untuk MWCNTs julat dari 0% hingga 1% berat. Nanokomposit PUs yang disintesiskan telah dicirikan mengikut ciri-ciri fizikal yang berbeza seperti mekanikal, perubahan morfologi dan kestabilan terma oksidatif dan juga ketulenan sampel dan luas permukaan; dengan menggunakan Fourier Transform Infrared Spektroskopi (FTIR), Pancaran Medan Mikroskopi Elektron Pengimbasan (FESEM), pembelauan sinar-x (XRD), analisis termogravimetri (TGA) dan kalorimetri imbasan pembeza (DSC). Luas permukaan dikaji oleh teknik Brunauer-Emmet-Teller (BET) dan nisbah unsur telah disiasat oleh analisis tenaga serakan sinar-x (EDX) dengan peralatan yang digabungkan bersama FESEM. Ciri-ciri halangan telah disiasat oleh ukuran kebolehtelapan nitrogen menggunakan unit pemisahan membran. Pertambahbaikkan yang besar bagi sifat-sifat terma dan mekanikal matriks COPUs telah didapati dengan menggabungkannya bersama tanah liat organo dan MWCNTs. Keserasian MWCNTs tulen telah terbukti lebih tinggi berbanding keserasian tanah liat organo di dalam matriks polimer walaupun pada kepekatan MWCNTs yang rendah (0.3%) menunjukkan jarak d yang lebih tinggi, sifat mekanikal dan sifat haba seperti yang ditunjukkan dalam analisis memainkan peranan yang berbeza, berbanding tanah liat organo seumpamanya (3% berat). Sifat tegangan menunjukkan peningkatan sebanyak 324% ~ dalam kekuatan tegangan dan penurunan sebanyak ~ 74% dalam pemanjang memutus dengan 5% berat tanah liat organo, manakala nanokomposit COPUs - MWCNTs menunjukkan satu perkembangan besar dalam kekuatan tegangan dan menurunkan nilai pemanjangan memutus dengan 1% berat (~640% dan ~ 80%). Sifat haba menunjukkan peningkatan sebanyak 10-30 ºC dalam COPUs - nanokomposit C30B, manakala peningkatan yang ketara suhu degradasi sebanyak (~ 50 ºC) diperhatikan dengan 0.3% berat MWCNTs didalam matriks COPUs. Pengurangan nilai kebolehtelapan yang besar (~ 25% dan 50% ~) dicapai dengan 5% berat daripada tanah liat organo dan nanokomposit bermuatan 0.5% berat MWCNTs, dengan COPUs tulen. Kajian pengoptimuman telah dijalankan oleh kaedah gerak balas permukaan (RSM), termasuk reka bentuk komposit pusat (CCD) dengan tiga faktor; suhu, masa dan jumlah bahan pengisi nano. Peningkatan suhu dan jumlah bahan pengisi nano mempengaruhi pempolimeran nanokomposit sehingga ke tahap tertentu. Kekuatan tegangan optimum yang diperolehi ialah (1,997 MPa pada suhu 90 ºC dan wt% 4.99%) untuk tanah liat dan (2,207 MPa pada suhu 90 ºC dan wt% 1%) untuk MWCNTs.

TABLE OF CONTENTS

Page

SUPERVISORS' DECLARATION ii
STUDENT'S DECLARATION iii
ACKNOWLEDGEMENTS v
ABSTRACT vi
ABSTRAK vii
TABLE OF CONTENTS viii
LIST OF TABLES xiv
LIST OF FIGURES xvii
LIST OF SYMBOLS xxvii
GREEK SYMBOLS xxvii
LIST OF ABBREVIATIONS xxviii

CHAPTER I INTRODUCTION

1.1 Motivation 1
1.2 Problem statement 5
1.3 Research objectives 6
1.4 Scope of research 7
1.5 Novelty of the work 7
1.6 Research contribution 8
1.7 Summary of Chapters 9

CHAPTER II LITERATURE REVIEW

2.1 Introduction 11
2.2 Polyurethanes 13
  2.2.1 Properties of polyurethane 15
  2.2.2 Application of polyurethane 15
  2.2.3 Synthesis of polyurethane 16
  2.2.3.1 Based on petrochemical polyol 17

2.2.3.2 Based on castor oil 19

2.3 Types of Isocyanate 21

2.3.1 Reaction of isocyanate 24
(i) Primary reactions of isocyanates 24
(ii) Secondary reactions of isocyanates 25
2.4 Polymer Nanocomposites 26
2.5 Nanofillers 29
2.5.1 Polyurethane Organoclay nanocomposites 30
2.5.1.1 Structure and properties of layered silicate 31
2.5.1.2 Modification techniques of layered silicates 34
2.5.2 Carbon Nanotubes (CNTs) 36
2.5.2.1 Properties of CNTs 37
2.5.2.2 Modification technique of CNTs 40
2.5.2.3 Carbon Nanotube-Polymer Nanocomposites 40
2.6 Structure of polymer nanocomposites 41
2.7 Preparation methods of polymer nanocomposites 42
2.7.1 Solution Intercalation 43
2.7.2 Melt Intercalation 44
2.7.3 In Situ Polymerization 46
2.7.3.1 Organo-Clay 49
2.7.3.2 Carbon Nanotubes 53
2.8 Mechanical properties of polyurethane nanocomposites 56
2.8.1 Tensile Testing 59
2.9 Thermals properties of polyurethane nanocomposites 60
2.10 Barrier properties of polyurethane nanocomposites 63
2.11 Optimization of the synthesis of polyurethane nanocomposites 64
2.12 Summary 67

CHAPTER III METHODOLOGY

3.1 Introduction 68

3.2 Materials 69

3.2.1 Toluene Diisocyanate (TDI) 69

3.2.2 Polyols 69

3.2.3 Castor Oil 70

3.2.4 Chain Extender 71

3.2.5 Nanofillers 72

(i) Organo-Clays 72

(ii) Carbon Nanotubes (CNTs) 72

3.2.6 Catalysts 73

3.3 Set up of synthesis rig 73

3.4 Synthesis of pure polyurethane, neat polyurethane based castor oil, polyurethane - organoclay and polyurethane – MWCNTs nanocomposites. 75

3.4.1 Synthesis of pure polyurethane 75

3.4.2 Synthesis of polyurethane based castor oil 75

3.4.3 Synthesis of polyurethane organic clay nanocomposite 77

3.4.4 Modification of MWCNTs 79

3.4.5 Synthesis of polyurethane carbon nanotubes nanocomposites 81

3.5 Characterization of polyurethane nanocomposite and analytical techniques 82

3.5.1 Fourier Transform Infrared Spectroscopy (FT-IR) Analysis 83

3.5.2 X-ray Diffraction (XRD) analysis 85

3.5.3 Microscopy Techniques 87

3.5.3.1 Scanning Electron Microscopy (SEM) 88

3.5.3.2 Field Emission Scanning Electron Microscopy (FESEM) 89

3.5.4 Thermal behaviour of polyurethane nanocomposite 91

3.5.4.1 Thermogravimetric Analysis (TGA) 91

3.5.4.2 Differential Scanning Calorimetry (DSC) 93

3.5.5 Brunauer-Emmet-Teller (BET) surface area technique 94

3.5.6 Mechanical testing 96

3.5.6.1 Tensile testing 96

3.5.7 Barrier properties of polyurethane nanocomposite 98

3.6 Optimization of polyurethane nanocomposites using Response Surface Methodology (Rsm) 101

3.6.1 Experimental design with RSM 101

3.7 Summary 102

CHAPTER IV RESULTS AND DISCUSSION

4.1 Introduction 104

4.2 Physico-Chemical properties of pure polyurethane and polyurethane based castor oil 105

4.2.1 Morphological studies of pure PUs and COPUs 105

4.2.1.1 Fourier Transform Infrared Spectroscopy (FTIR) studies 105

4.2.1.2 X-ray diffraction (XRD) of polyurethane studies 106

4.2.1.3 Scanning Electron Microscope (SEM) studies 107

4.2.2 Synthesis mechanism 108

4.2.2.1 Synthesis mechanism of pure polyurethanes 108

4.2.2.2 Synthesis mechanism of castor oil based polyurethanes 109

4.2.3 Mechanical properties of polyurethane studies 110

4.2.4 Thermal stability studies 111

4.2.4.1 Thermogravimetric analysis (TGA) 111

4.2.4.2 Differential scanning calorimetry (DSC) 114

4.3 Synthesis of polyurethane based castor oil organoclay nanocomposites 115

4.3.1 Morphologies studies of COPUs – C30B nanocomposites 115

4.3.1.1 Fourier Transform Infrared Spectroscopy (FTIR) studies 115

4.3.1.2 X-ray diffraction (XRD) of polyurethane-organoclay nanocomposites studies 120

4.3.1.3 Field emission scanning electron microscope (FESEM) studies 123

4.3.1.4 Element detection analysis studies 124

4.3.2 Synthesis mechanism of COPUs-CB30 nanocomposites 126

4.3.3 Mechanical properties of COPUs-C30B nanocomposites film 126

4.3.4 Thermal stability studies 128

4.3.4.1 Thermogravimetric analysis (TGA) studies 128
4.3.4.2 Differential scanning calorimetry (DSC) 133
4.3.5 Gas-barrier properties of COPUs-C30B nanocomposites 135
4.3.6 BET surface analysis 137
4.4 Synthesis of polyurethane based castor oil-MWCNTs nanocomposites 138
4.4.1 Purification of raw MWCNTs 138
4.4.2 Morphologies studies of COPUs – MWCNTs nanocomposites 140
4.4.2.1 Fourier Transform Infrared Spectroscopy (FTIR) studies 140
4.4.2.2 X-ray Diffraction (XRD) studies 144
4.4.2.3 Field Emission Scanning Electron Microscope (FESEM) studies 147
4.4.2.4 Element detection analysis studies 149
4.4.3 Synthesis mechanism 150
4.4.4 Mechanical properties studies 151
4.4.5 Thermal stability studies 152
4.4.5.1 Thermogravimetric analysis (TGA) studies 152
4.4.5.2 Differential scanning calorimetry (DSC) 158
4.4.6 Gas-barrier properties studies 160
4.4.7 BET surface analysis 162
4.5 Comparative Study of Organoclay and Multiwalled Carbon Nanotubes (MWCNTs) on Physico-Chemical Behaviour of Castor Oil Based Polyurethanes 163
4.5.1 Morphologies studies of COPUs-C30B and COPUs-MWCNTs nanocomposites 163
4.5.1.1 Fourier Transform Infrared Spectroscopy (FTIR) studies 163
4.5.1.2 X-ray Diffraction (XRD) studies 164
4.5.1.3 Field Emission Scanning Electron Microscope (FESEM) studies 166
4.5.2 Mechanical properties studies 167
4.5.3 Thermogravimetric analysis (TGA) studies 169
4.6 Summary 170

CHAPTER V OPTIMIZATION

5.1 METHOD 172
5.1.1 Experimental design with RSM for COPUs - C30B nanocomposites 172
5.1.2 Response Surface Method (RSM) 173
5.1.2.1 Adequacy check of model 176
5.1.2.2 Diagnostics of case studies 176
5.2 Optimization Condition for Response Surface Analysis 180
5.2.1 Model validation and experimental confirmation 182
5.3 Experimental design with RSM for COPUs-MWCNTs nanocomposites 183
5.3.1 Response Surface Method (RSM) 185
5.3.1.1 Adequacy check of the model 187
5.3.1.2 Diagnostics of the case studies 187
5.4 Optimization Condition for Response Surface Analysis 191
5.4.1 Model validation and experimental confirmation 193
5.5 Summary 194

CHAPTER VI CONCLUSION AND RECOMMENDATIONS

6.1 Conclusion 196
6.2 Recommendations for Future Research 199
References 201
Appendix A 237
Appendix B 246

LIST OF TABLES

Table No.	Title	Page
2.1	Common diisocyanates used for the production of polyurethanes	22
2.2	Clay mineral (phyllosilicate) classification	33
2.3	Chemical formula and characteristic parameter of commonly used 2:1 phyllosilicates	34
2.4	Theoretical and experimentally measured properties of CNTs	38
3.1	Physical properties of TDI	70
3.2	Properties of Polypropylene Glycol	70
3.3	Composition of castor seed oil /fatty acid chains	71
3.4	Physical properties of castor oil	71
3.5	Properties of 1-4-butanediol	72
3.6	Properties of Cloisite B30	73
3.7	Factors and respected ranges decided for the screening experiment	101
4.1	XRD data for pure PUs and COPUs	106
4.2	Results from TG and DTG curves of pure PUs and COPUs	113
4.3	Crystallinity percentages of pure PUs and COPUs	115
4.4	The characteristic bands in the IR spectra obtained of C30B	116
4.5	The characteristic bands in the IR- spectra obtained from COPUs	117
4.6	The characteristic bands in the IR- spectra obtained from COPU-C30B nanocomposites	117
4.7	XRD data for COPUs and COPU-C30B nanocomposites with different weight percentages of organoclays	121

4.8 EDX studies of different weight (%) of organo-clay in COPU matrix with elemental weight and atomic percentages 125

4.9 Weight loss % during thermal decomposition of neat COPUs and COPU-C30B nanocomposites with different C30B wt% 130

4.10 Results from TG and DTG curves of the COPUs and COPUs-C30B nanocomposites 131

4.11 Results from DSC curves of the soft segments and hard segment multiblock neat COPUs and COPU-C30B nanocomposites 134

4.12 Crystallinity percent of neat COPUs and COPU-C30B nanocomposites 135

4.13 The characteristic bands in the IR- spectra obtained from purified MWCNTs 140

4.14 The characteristic bands in the IR- spectra obtained of COPUs–MWCNTs nanocomposites 142

4.15 XRD data for neat COPUs and COPU-MWCNT nanocomposites with different percentages of MWCNTs 145

4.16 EDX studies of different weight% of MWCNTs in COPU matrix with elemental weight and atomic percentages 150

4.17 Decomposition and variation in temperatures for different weight (%) COPU-MWCNT nanocomposites 155

4.18 Weight loss during thermal decomposition of neat COPUs and COPU-MWCNTs nanocomposites with different MWCNT wt% 157

4.19 Results from DSC curves of the soft and hard segments for neat COPUs and COPU-MWCNT nanocomposites 160

4.20 Crystallinity percentages of neat COPUs and COPU-MWCNT nanocomposites 160

4.21 XRD data for neat COPUs, COPU-C30B and COPU-MWCNT nanocomposites 165

4.22 Stress and strain values of different nanocomposites 168

5.1 Factors and respected ranges decided for the screening experiment 172

5.2 Experimental results of dependent variable as polyurethanes-clay synthesis 174

5.3	Analysis of variance table exhibits individual as well as interaction effects	175
5.4	Statistical summary of screening results	175
5.5	Optimum condition obtained from RSM	183
5.6	Factors and respected ranges decided for the screening experiment	184
5.7	Experimental results of dependent variables as polyurethanes–CNT synthesis	185
5.8	Analysis of variance exhibits individual as well as interaction effects	186
5.9	Statistical summary of screening results	186
5.10	Optimum condition obtained from RSM	194

LIST OF FIGURES

Figure No.	Title	Page
2.1	Reaction mechanism of synthesis of polyurethanes using the prepolymer method	17
2.2	Schematic representation of a PU polymer chain with distinct hard (HS) and soft (SS) segments	18
2.3	Reaction mechanisms of different chemical reaction types of isocyanate	23
2.4	Reaction mechanisms of the resonance structures of the isocyanates	23
2.5	Reaction mechanisms of isocyanates with hydrogen active compounds	23
2.6	Reaction mechanism of polyurethane-links synthesis	24
2.7	Reaction mechanism of diisocyanates with amines	24
2.8	Reaction mechanism of diisocyanates with water	25
2.9	Secondary reaction mechanisms of isocyanates with hydrogen active atoms	25
2.10	Reaction mechanism of secondary reactions of self-polymerization isocyanates	26
2.11	Schematic diagram showing the three components involved for polymer nanocomposite fabrication	27
2.12	Structure of the 2:1 layered silicates	32
2.13	The cation-exchange process between alkylammonium ions and cations initially intercalated between the clay layers	35
2.14	Types of carbon nanotube	36
2.15	Schematic diagram of CNTs chirality from graphite sheet folding	39

2.16 Schematic diagrams of the three polymer modified layered silicate nanocomposites 42

2.17 The intercalation of polymers using the “solution” approach 43

2.18 The “melt intercalation” process 45

2.19 Schematic presentations of different steps of the “in-situ polymerisation” approach 47

2.20 Schematic representation of the in situ polymerization method 48

2.21 Nylon-6 nanocomposite formed through in-situ polymerization with ADA-MMT 48

2.22 Schematic representation of the (a) Chemical structure of organo-clay (Cloisite 30B) and (b) Hydrogen bonding of an organo-clay (Cloisite 30B) - tethered polyurethane chain 51

2.23 Studying the effects of (A) different dispersing agents (a) no dispersing agent, (b) BYK-985, (c) BYK-9076, (d) BYK-9077 (B) different mixing methods (a) stirring, and (b) ball milling 53

2.24 Scanning Electron micrographs (SEM) images of cross section of PU-MWNT composites: (a) PU-MWNT1, (b) PU-MWNT3, and (c) PU-MWNT2 54

2.25 Stress-strain curves for (a) the pure polyurethane and (b) as a polyurethane - clay nanocomposite prepared from C18A-SWy montmorillonite with 5 wt% 57

2.26 Stress-strain curves of PUs-organo hectorite clay nanocomposites 58

2.27 Tensile mechanical properties test sample according to ASTM D638-03 type I. 60

2.28 % mass conservation and derivative dependency on temperature for TPUs and TPUs nanocomposites 61

2.29 Thermograms of castor oil based chain extended polyurethane and polyurethane clay nanocomposites with varying percentages of clay 62

2.30 The Schematic representations of the ‘tortuous path’ through (a) a conventional composite and (b) a nanocomposite 63

3.1 Reactor assembly for in-situ polymerization synthesis 74

3.2 Set up of the curing of film by vacuum oven 76

3.3 Prepared COPU thin film 77

3.4 Dispersed of nanofillers in polyol by ultrasonication bath set up 78

3.5 Prepared COPUs/organo-clay nanocomposites thin film 79

3.6 MWCNTs purified via stirring acid treatment 80

3.7 High rpm centrifuged machine 81

3.8 Prepared COPU-MWCNT nanocomposite thin film 82

3.9 (a) The FTIR spectra were recorded using an FTIR Spectrophotometer (Nicolet 5DX FT- IR, USA) in the UMP Lab, (b) Schematic representation of a FTIR spectrometer 84

3.10 (a) The X-ray diffraction (XRD) patterns were recorded using an X-ray diffractometer (Rigaku Miniflex II, Japan) employing graphite monochromator and CuKα radiation (λ = 0.15406 nm) in the UMP Lab, (b) Schematic principle of X- ray Diffractometer 86

3.11 The Scanning Electron Microscope (SEM) 88

3.12 (a) The Field emission scanning electron microscope (FESEM) in UMP Lab, (b) Schematic of Field emission scanning electron microscope (FE-SEM), showing optical path of light 90

3.13 (a) The Thermogravimetric analysis (TGA) in UMP Lab, (b) Schematic representation of Thermogravimetry (TG) technique: instrumentation and working 92

3.14 Differential Scanning Calorimetry (DSC) 94

3.15 (a) Surface Analysis (ASAP 2020, Micromeritics, USA), (b) Schematic representation of BET surface area studies: technique, instrumentation and working 95

3.16 Tensile test specimen according to ASTM D-638-M-3 97

3.17 (a) Universal tensile testing machine in the UMP lab, (b) Tensile test specimen during a test 97

3.18 Mechanism of the barrier properties (a) before the addition of nanofillers and (b) after the addition of nanofillers 99

3.19 Image for gas permeability measurement shows the sample before testing 99

3.20 (a) Image for the gas permeability measurement system in the UMP Lab, (b) Diagram of gas permeability measurement 99

4.1 Comparative FTIR spectra for PUs (pure PPG & PPG and castor oil) 106

4.2 Comparative XRD graph for pure PUs and COPUs 107

4.3 SEM for PUs (a) without, and (b) with Castor Oil 108

4.1 Schematic representation of pure PUs synthesis mechanism using pre-polymer technique 109

4.2 Schematic representation of synthesis mechanism of neat COPUs using pre-polymer technique 109

4.4 Stress-strain curves for pure PUs and COPUs 110

4.5 Tensile strength of pure PUs and COPUs with 15wt% of castor oil 111

4.6 Comparative TGA graph for PUs (pure PPG & PPG and castor oil) 112

4.7 DTG curves of COPUs and pure PUs 113

4.8 DSC heating curves of pure PUs and COPUs 114

4.9 FTIR spectra of organoclay (Closite 30B) and COPUs 116

4.10 FTIR spectra of COPUs and COPU-C30B nanocomposite with different percentages of organoclays 118

4.11 Comparative FTIR spectra of COPUs and COPU-C30B nanocomposites (1, 3, and 5 %) organoclays, with a wavelength range of 1250 to 1800 cm^{-1} 119

4.3 The interference of organoclay layers on hydrogen bonding in polyurethane composites 119

4.12 XRD of C30B, neat COPUs and COPU-C30B nanocomposites with varying wt % of organoclay loading 121

4.13 XRD of organoclay (C30B), neat COPUs and COPU-C30B nanocomposites with varying percentages of organoclay 122

4.14 Machine originated graph for 5wt% COPU-C30B nanocomposites 122

4.15 The surface FESEM images of pristine COPUs and nanocomposites in different weight percentages of 1, 3 and 5 wt% organoclay (Cloisite 30B) 123

4.16 EDX analysis of COPUs/organo-clay nanocomposites 125

4.4 Schematic representation of the synthesis of COPU-C30B nanocomposites using in-situ polymerization 126

4.17 Stress strain curves for pure COPUs and COPU-C30B nanocomposites with varying percentages of organoclay loading 127

4.18 Tensile strength of COPUs and COPU-C30B nanocomposites with 1, 3 and 5 wt% organoclay 128

4.19 TGA spectrum of castor oil based polyurethanes, both pure and COPUs with changing wt% of organoclay (Cloisite 30B) nanocomposites 129

4.20 DTG curves of COPUs and COPU-C30B nanocomposites with varying % of organoclay loading 132

4.21 Weight loss percentage of neat COPUs and COPU-C30B nanocomposites with different C30B wt% at 400 ^{o}C 133

4.22 DSC heating curves of neat COPUs and COPU-C30B nanocomposites films 134

4.23 Nitrogen permeability percentage rate vs organoclay wt% 136

4.24 Hypothetical model describing the path of diffusing N_2 gas through the COPU-organoclay nanocomposite. (d) Actual distance travelled in the absence of fillers, (d') tortuous path length in the presence of fillers 137

4.25 Nitrogen adsorption-desorption isotherms of 5 wt% COPU-organoclay 138

4.26 FTIR spectrum of raw MWCNTs and purified MWCNTs 139

4.27 XRD spectra graph of raw MWCNTs and purified MWCNTs 139

4.28 FTIR spectra of purified MWCNTs and COPUs 141

4.29 FTIR spectra of pure COPUs and COPU-MWNT nanocomposites, with varying 0.1, 0.2, 0.3, 0.4, 0.5, and 1 wt% MWCNT loadings 142

4.30 FTIR spectra of COPUs and (COPUs-MWCNTs) nanocomposite with different percentages of MWCNTs, wavelength ranges from 1450 to 1800 cm^{-1} 143

4.5 Hydrogen bonding within polyurethane purified MWCNT nanocomposites 144

4.31 X-ray diffraction patterns of COPUs and the purified MWCNTs 145

4.32 Powder X-ray diffraction patterns of pure COPUs and the COPU-MWCNT nanocomposites with virgin 0.1, 0.2, 0.3, 0.4, 0.5 and 1 wt% MWCNTs loadings 146

4.33 FESEM images of fractured surface of (a) 0% MWCNTs, (b) 0.2% MWCNTs, and (c) 0.3% MWCNTs in COPUs matrix 148

4.34 FESEM images of fractured surface of (a) 0.5% MWCNTs, and (b) 1% MWCNTs, in COPUs matrix 148

4.35 EDX analysis of COPU-MWCNT nanocomposites 149

4.6 Schematics representation of synthesis mechanism of COPU-MWCNT nanocomposites’ with in situ polymerization method 150

4.36 Stress-strain curves of pure COPUs and COPU-MWCNT nanocomposites with various 0.3, 0.5, and 1 wt% MWCNT loadings 151

4.37 Tensile strength of COPUs and COPU-MWCNT nanocomposites with varying 0.3, 0.5, and 1 wt% MWCNT loadings 152

4.38 TGA spectrum of pure COPUs and COPU-MWCNT nanocomposites with varying degrees of MWCNT wt% (0.1, 0.2, 0.3, 0.4, 0.5, and 1) 151

4.39 TGA spectrum of pure COPUs and COPU-MWCNT nanocomposites with varying MWCNT wt% (0.1, 0.2 and 0.3) 154

4.40 TGA spectrum of pure COPUs and COPU-MWCNT nanocomposites with varying MWCNT wt% (0.4, 0.5 and 1) 154

4.41 DTG curves of COPUs and COPU-MWCNT nanocomposites with varying % of MWCNTs 0, 0.1, 0.2 and 0.3 wt% 156

4.42 DTG curves of COPUs and COPU-MWCNT nanocomposites with varying % of MWCNTs 0.4, 0.5 and 1 wt% 156

4.43 Weight loss percentage of neat COPUs and COPU–MWCNT nanocomposites with different MWCNT wt% at 400 °C 158

4.44 DSC heating curves of neat COPUs and COPU-MWCNT nanocomposites films 159

4.45 Nitrogen permeability rates in different MWCNT weight percentages 161

4.46 Hypothetical model describing the path of the diffusing N_2 gas through the COPU-MWCNTs nanocomposite. (d) Actual distance travelled in the absence of fillers, (d’) tortuous path length in the presence of fillers 163

4.47 Nitrogen adsorption-desorption isotherms of 0.5 wt% COPU-MWCNTs 163

4.48 FTIR spectra of neat COPUs, COPU-C30B nanocomposites at 3wt%, and COPU-MWCNT nanocomposites at 0.3wt% 164

4.49 X- ray diffraction plots of COPUs, COPU-C30B nanocomposites at 3wt% and COPU-MWCNT nanocomposites at 0.3wt% 165

4.50 The FESEM images of the surfaces of COPUs and COPU-C30B nanocomposites at 3wt% and COPU-MWCNT nanocomposites with 0.3wt% 167

4.51 Stress strain curves for COPUs, COPUs - C30B nanocomposite with 3wt% and COPUs - MWCNTs nanocomposite with 0.3wt%. 168

4.52 TGA spectrum of castor oil based on polyurethanes neat COPUs, COPUs - C30B nanocomposite with 3wt% and COPUs – MWCNTs nanocomposite with 0.3wt% 169

4.53 DTG curves of COPUs and COPUs - C30B nanocomposites with 3% and COPUs - MWCNTs with 0.3% nanocomposites loading 170

5.1 Normal plot of residuals generated from the model 177

5.2 Dignostic plot generated from the model for plot of Residual vs Predicted 178

5.3 Dignostic plot generated from the model for plot of Residual vs Run Number 178

5.4 Design-expert plot; predicted vs. actual values plot for tensile strength 179

5.5 Box-Cox plot for power transforms 179

5.6 3D plot - Interaction of clay amount and time 180

5.7 3D plot - Interaction of clay amount and temperature 181

5.8 3D plot - Interaction of time and temperature 182

5.9 Normal plot of residuals generated from the model 188

5.10 Dignostic plot of residual vs predicted 189

5.11 Dignostic plot of residual vs run number 189

5.12 predicted vs. actual values plot 190

5.13 Box-Cox plot for power transforms 190

5.14 3D plot - Interaction of CNTs amount and time 191

5.15 3D plot - Interaction of CNTs amount and temperature 192

5.16 3D plot - Interaction of time and temperature 193

NOMENCLATURES

List of Symbols

Symbol	**Meaning**
K	Kelvin
^{o}C	Degree Celsius
HS	Hard segments
SS	Soft segments
NL	Nitrolignin
Pa	Pascal
T_g	glass transition temperature
CEC	Cation exchange capacity
D	Interlayer spacing
MPa	Mega Pascal
ASTM	American Society for Testing and Materials
GA	genetic algorithms
DMF	Dimethyl formamide
X_c	Crystallinity index
ΔH_f	Heat of fusion of the sample
F	Force
Å	Angstrom

Greek Symbols

Symbol	**Meaning**
l	Length
ε	Strain
σ	Stress
τ	Tortuosity
α	Aspect ratio
λ	Wavelength
θ	Angle
$\mathcal{E}$	The residual term.
δ	Bath difference
e	extension

LIST OF ABBREVIATIONS

CNTs	Carbon nanotubes
Pus	Polyurethanes
MMT	Montmorillonite
CO	Castor oil
COPU	Castor oil based polyurethane
COPUs	Castor oil based polyurethanes
C30B	Cloisite B30
MWCNTs	Multi-Walled Carbon Nanotubes
TDI	Toluene diisocyanate
Rpm	Revolutions per minute
EPUs	Epoxy-terminated polyurethanes prepolymers
HDI	Hexamethylene diisocyanate HDI
COFPL	Castor oil-based flame retardant polyols
MDI	Diphenylmethane diisocyanate
TPU	Thermoplastic polyurethane
PPG	Polypropylene glycol
PEG	Polyethylene glycol
PEI	Poly ethylene imine
SWCNT	Single walled carbon nanotube
TGA	Thermo-gravimetric analysis
BET	Brunauer-Emmet-Teller
RSM	Response surface methodology
EDX	Energy Dispersive X-ray spectroscopy

XRD	X-ray diffraction
DSC	Differential scanning calorimetry
FESEM	Field Emission Scanning Electron Microscopy
SEM	Scanning Electron Microscope
NTs	Nanotubes
ADA	Aminododecanoic acid
PC-PUs	Polycarbonate-based polyurethanes
PCL	Poly (ε-caprolactone)
BDO	Butane diol
PS	polystyrene

CHAPTER I

INTRODUCTION

1.1 MOTIVATION

In the past five decades, polymer/filler nanocomposites have attracted great interest, both in industry and academia for a wide range of applications due to its remarkable improvements in material properties at very fine level with low nano filler loading when compared to virgin polymer or conventional composites (Rajkumar *et al*., 2013). Polymers filler composites have been widely used as a method of improving physico-chemical properties. These enhancements can include increased strength, heat resistance (Lahorija *et al*., 2010; Papageorgiou *et al*., 2013 and Rajkumar *et al*., 2011), and decreased gas permeability (Ruijian et al., 2003; Pradip et al., 2010 and Morteza et al., 2011). The main difficulty in the synthesis of polymer nanocomposites is the ability to achieve uniform dispersion of nanofillers in the polymer matrix (Behdad *et al*., 2013). The three levels of dispersion are conventional composites, intercalated or partially exfoliated nanocomposites and fully exfoliated nanocomposites (Musa *et al*., 2010). The field thrived after a research finding was presented by the Toyota Research Group (Kojima, 1993; Jeffrey and Tkashik, 1997 and Edcleide, 2011) in the 90s on unfamiliar physical property enhancements in a nylon 6/clay nanocomposite when integrated with minimal amount of filler loading. Light weight and economic competitiveness usage of only a minimal amount of reinforcing materials, usually below 5 wt%, represent other key advantages of organic-inorganic nanocomposites (Samira *et al*., 2014). The ultimate polymer nanocomposites are shaped when nanofillers are completely dispersed into a polymer matrix and interact well between the polymer matrix and the surface of modified nanofillers. A high energy sonication process and mixing assisted by high energy shear force is an effective method to improve particle distribution (Kiliaris, 2010 and Daniel *et al*., 2013). This structure refers to the exfoliated system which yields maximum improvement in properties. However, in many cases, the nanocomposites reported tend to become intercalated or partially exfoliated. Sometimes in an exfoliated structure, nanofillers are randomly dispersed in polymer chains to achieve improvements in physico-chemical properties (Onal *et al*., 2006).

In recent years, development of nanocomposites has been widened into almost every engineering polymer including polypropylene (Monica *et al*., 2010), polyethylene (Bergaya *et al*., 2005), polystyrene (Xaoan *et al*., 1999; Peter *et al*., 1999 and Dirk *et al* 2006), polyvinylchloride (Chaoying *et al*., 2003), acrylonitrile butadiene styrene (Modesti *et al*., 2007), polymetylmethacrylate (Utracki *et al*., 2010), polyethylene terephatalate (Guozhen *et al*., 2002), ethylene-vinyl acetate copolymer (Hyung *et al*., 2007), polyacrylonitrile (Yagoub *et al*., 2012), polycarbonate (Saptarshi *et al*., 2012), polyethylene oxide (Burgaz, 2011), epoxy resin (Ole *et al*., 2002), polyimide (Chyi *et al*., 2003), polylactide (Barrau *et al*., 2011), polycaprolactone (Hongdan *et al*., 2010), phenolic resin (Shiao *et al*., 2006), poly p-phenylene vinylene (Anupama *et al*. 2010), polypyrrole (Zhanhu *et al*., 2009), rubber (Yiqing *et al*., 2005), polyurethane (Song *et al*., 2006; Yusoh, 2010 and Aranguren *et al*., 2012), urethane alkyd (Saravari *et al*., 2013)and polystyrene (Huating *et al*., 2010).

The transition from microparticles to nanoparticles can dramatically change the physical properties (Ryszkowska, 2008). A critical advantage of polymer nanocomposites over old-fashioned bulk composites is that the nano sized fillers lead to an intense increase in interfacial area, opening gateways to new applications (Schadler *et al*., 2007). Materials at the nano scale, exhibits diverse properties due to higher surface area and new quantum effects. Greater surface area to volume ratio with respect to conventional forms, lead to superior chemical reactivity and improved material mechanical performance (Lijie and Thomas, 2009). The results showed that nanostructured materials can have extensively diverse properties compared to a larger-dimensional material of the similar composition (Hussain and Mehdi, 2006). The polymer nanocomposites types depend on its nanofillers, such as nanoparticles of organoclay, metal oxides, carbon nanotubes and graphene. Usually, the size and shape of particles have a major effect on the final properties of its polymer/inorganic nanoparticle nanocomposites (Muhammad, 2013).

The first study of mechanical properties enhancements by Okada *et al.*, originated from in-situ polymerized hybrid organic and inorganic nanocomposites (Okada and Usuki, 1995; Giannelis, 1996 and Ogawa and Kuroda, 1997). The main issue is the important chemical and physical interactions that are directed by surfaces and surface properties. Nanostructured material can have substantially dissimilar properties from larger-dimension materials of the same composition (Mohammed, 2012). Polymer composite performances can be enhanced such as increase in tensile strength and decrease in gas permeability and tear strength without losing elasticity can be enhanced depending on the type and amount of fillers as well as the level of intercalation or exfoliation of fillers in polymer matrix (Nanying *et al.*, 2008 and Paul *et al.*, 2013). The use of nanofillers has become abundant in polymeric synthesis. Carbon nanotubes (CNTs) and organoclay are the most widely used material in academia and industrial laboratories all over the world to formulate polymer nanocomposites (Christopher *et al.*, 2013 and Yong *et al.*, 2013). Polyurethanes (PUs) are among the most important polymeric materials, with distinctive physical and chemical properties that are flexible, highly mechanical, and have thermal and chemical resistances (Yusoh 2010 and Akintayo, 2013). PUs can be tailored to meet the diversified demands of various applications such as rigid insulations, coatings, footwear adhesives (Saraswathy, 2009 and Jessica and Jose, 2011), thermoplastic elastomers and foams, as well as medical devices (Golaz *et al.*, 2011; Liqiang *et al.*, 2014 and Xuefeng *et al.*, 2014). A wide range of fillers, modified clays and CNTs with structural modifications are used in the synthesis of polymer - fillers nanocomposites (Chattopadhyay *et al.*, 2007).

Recently, a large number of polymer nanocomposite matrices have been synthesized and significant enhancements in composite properties have been reported (Dilini *et al.*, 2012). The first polymer-clay nanocomposite was reported in 1961, when Blumstein polymerized vinyl monomers intercalated in Montmorillonite (MMT) (Blumstein, 1961 and Dirk, 2006). Oriakhi in 1998 stated that ‘Nature is a master chemist with incredible talent’, showing that by using natural reagents and polymers such as carbohydrates, lipids, and proteins (Oriakhi, 1998), nature makes strong

CHAPTER III

METHODOLOGY

3.1 INTRODUCTION

This chapter focuses primarily on the synthesis of polyurethanes for pure as well as with nanofillers (modified organoclay and MWCNTs) integrated in the PUs matrix to form nanocomposites. In the other half of the chapter, a brief and comprehensive description of analytical instruments which were employed in a comparative study of physicochemical properties of pure PUs and filler incorporated polymer-filler nanocomposites is discussed. Nanocomposites of PUs have heightened importance in wide scale applications during the last decade due to their improved properties over conventional composites. Due to the large consumption of PUs and the negative environmental impacts from petroleum based polyols, renewable resources as alternative materials are now of great interest to researchers. Castor oil, one of the major non-edible vegetable oils is an interesting renewable resource that contains a hydroxyl group (-OH) and unsaturated double bonds (C=C) in its organic chain, and is able to produce new polyurethane materials. The synthesis methodology encompass three different syntheses, which includes pure PUs with no fillers incorporated, PU/organoclay (Cloisite B30) nanocomposites and new PU/multi-walled carbon nanotube (MWCNT) nanocomposites which employs a mixture ratio of polypropylene glycol and castor oil as polyols.

The crystal structure was studied using X-ray diffraction (XRD). The XRD patterns were recorded using an X-ray diffractometer (*Rigaku* Mini Flex II, Japan) which employs graphite monochromator and CuKα radiation ($\lambda = 0.15406$ nm). The morphology was examined using Scanning electron microscopy (SEM) on the JEOL 6300F (Japan) machine at an acceleration voltage of 5KV and field emission scanning electron microscopy (FESEM, *JEOL EVO-50, Japan*). Infrared absorption spectroscopy (IR) spectrum was measured at room temperature using a Fourier transform infrared (FTIR) spectrometer (*Nicolet* 5DX FT-IR, USA). Thermal stability was tested usingThermo-gravimetric analysis (TGA) on a thermal analyzer (*Mettler Toledo*, TGA/DSC1) at a rate of 10 ^{o}C min^{-1} and on a Differential Scanning Calorimetry (DSC) model of TA- Instrument DSC/Q 1000 (V9.6, Build 290). BET surface area of the composite was studied using gas adsorption studies (ASAP 2020, *Micromeritics*, USA). Atomic percentages of elements in neat COPUs, organoclay and MWCNTs were calculated using Energy Dispersive X-ray spectroscopy (EDX) attached within FE-SEM. The study of mechanical properties (tensile strength and elongation at break) were carried out using an Instron model 4505 universal testing machine at 25 ºC with a load cell of 5 KN, followed by ASTM D 638. Crosshead speed was set to 2 mm/min. Samples were cut into dumbbell shapes using ASTM D 638 (type V).

3.2 MATERIALS

Major building-blocks for the synthesis of renewable polyurethanes are:

3.2.1 Toluene Diisocyanate (TDI)

In this research, Toluene diisocyanate (TDI) was used for the preparation of PU samples. TDI used as received was supplied from SIGMA-Aldrich Company. Its physical properties are shown in Table 3.1. TDI is an aromatic diisocyanvate.

3.2.2 Polyols

Polyols are defined as chemical compounds that contain more than one hydroxyl group (diol). Polyols are separated into two categories, which are low molecular weight and high molecular weight polyols. High molecular weight polyols called oligo-polyols, are one of the main building blocks that represents the soft segment in the formation of polyurethane.

Table 3.1: Physical properties of TDI.

Constituent	**value**
Commercial name	Toluene Diisocyanate (TDI)
Molecular formula	$C_9H_6N_2O_2$
Molecular weight	174.2
Appearance	White or pale yellow solid
Density	1.214 g/cm^3, liquid
Melting point	21.8 °C (295 K)
Boiling point	251 °C (524 K)
Solubility in water	Reacts

In this research, a polyether polyol (Polypropylene Glycol, Molecular weight = 4000) was supplied by Sigma-Aldrich Company and was selected as the soft segment. The details are shown in Table 3.2.

Table 3.2: Properties of Polypropylene Glycol.

Constituent	**value**
Commercial name	P 4000
Appearance	Colorless liquid
Molecular weight	4000
OHV	28 mg KOH/g
Viscosity (25 ^{o}C)	1300 mPa.s
Functionality	1.7
Structure	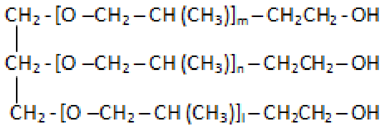 $CH_2-[O-CH_2-CH(CH_3)]_m-CH_2CH_2-OH$ $\vert$ $CH_2-[O-CH_2-CH(CH_3)]_n-CH_2CH_2-OH$ $\vert$ $CH_2-[O-CH_2-CH(CH_3)]_l-CH_2CH_2-OH$

3.2.3 Castor Oil

In this work, castor oil was used as an alternative to petrochemical based polyols and as a renewed resource that can potentially reduce cost in polyethane production. In this research, pure castor oil was purchased from Chengdu Organic Chemicals, China and polymerized directly without modifications. Table 3.3 shows the composition of castor oil, while Table 3.4 shows the properties of castor oil.